ALCAM contributes to brain metastasis formation in non-small-cell lung cancer through interaction with the vascular endothelium

Justine Münsterberg[1*] & Desirée Loreth[1*], Laura Brylka[2], Stefan Werner[1], Jana Karbanova[3], Monja Gandrass[1], Svenja Schneegans[1], Katharina Besler[1], Fabienne Hamester[4], José Ramon Robador[5,6], Alexander Thomas Bauer[5,6], Stefan Werner Schneider[6], Michaela Wrage[1], Katrin Lamszus[7], Jakob Matschke[8], Yogesh Vashist[9], Güntac Uzunoglu[9], Stefan Steurer[10], Andrea Kristina Horst[11], Leticia Oliveira-Ferrer[4], Markus Glatzel[8], Thorsten Schinke[2], Denis Corbeil[3], Klaus Pantel[1], Cecile Maire[7], Harriet Wikman[1]

1. Department of Tumor Biology, University Medical Centre Hamburg-Eppendorf, Hamburg, Germany
2. Department of Osteology and Biomechanics, University Medical Center Hamburg Eppendorf, Hamburg, Germany
3. Biotechnology Center (BIOTEC) and Center for Molecular and Cellular Bioengineering (CMCB), Technische Universität Dresden, Dresden, Germany
4. Department of Gynecology, University Medical Center Hamburg-Eppendorf, Hamburg, Germany
5. Experimental Dermatology, Department of Dermatology, Venereology, and Allergy, Medical Faculty Mannheim, University of Heidelberg, Mannheim, Germany
6. Department of Dermatology and Venerology, University Hospital Hamburg-Eppendorf, Hamburg, Germany
7. Department of Neurosurgery, University Medical Center Hamburg-Eppendorf, Hamburg, Germany
8. Department of Neuropathology, University Medical Centre Hamburg-Eppendorf, Hamburg, Germany
9. General, Visceral and Thoracic Surgery Department, University Medical Centre Hamburg-Eppendorf, Hamburg, Germany
10. Institute of Pathology, University Medical Center Hamburg-Eppendorf, Hamburg; Germany
11. Institute for Experimental Immunology and Hepatology, University Medical Center Hamburg-Eppendorf, Hamburg; Germany

*Shared first

Corresponding author:

Harriet Wikman, Ph.D.

Department of Tumor Biology,

University Medical Center Hamburg-Eppendorf,

Martinistraße 52, 20246 Hamburg, Germany

Phone: +49-40-7510 51913

Email: h.wikman@uke.de

Funding: This study was funded by the Deutsche Krebshilfe (German Cancer Aid), Priority Program "Translational Oncology", #70112507, "Preventive strategies against brain metastases" (DL, KP and

HW) and Deutsche Forschungsgemeinschaft (DFG), Priority Program SPP2084 (DC and HW). The Hamburger Krebsgesellschaft e.V. supported the study by providing a doctoral scholarship (JM).

Conflict of Interest: none

Authorship:

Study concept and design: JM, DL, SW, MW, HW

Data analysis: JM, DL, SW, JK, MGa, MW, CM, HW

Patient sample collection: JM, KL, JMa, YV, GU, SSt, MGl

Performed experiments: JM, DL, LB, SW, JK, MGa, SS, KB, FH, JA, LO-F, CM

Data Interpretation: JM, DL, LB. MGa, AB, SWS, AKH, TS, DC, CM, HW

Drafted manuscript: JM, DL, SW, KP, HW

Approved final manuscript: all authors

Word count: 6171

1. Abstract

Background. Brain metastasis in non-small cell lung cancer (NSCLC) has a very poor prognosis. Recent studies have demonstrated the importance of cell adhesion molecules in tumor metastasis. The aim of our study was to investigate the role of activated leucocyte cell adhesion molecule (ALCAM) in brain metastasis formation in NSCLC.

Methods. Immunohistochemical analysis was performed on 143 NSCLC primary tumors and brain metastases. A correlation between clinicopathological parameters and survival was developed. Biological properties of ALCAM were assessed *in vitro* by gene ablation using CRISPR/Cas9 technology in the NCI-H460 NSCLC cell line and *in vivo* by intracranial and intracardial cell injection of NCI-H460 cells in NMRI-*Foxn1*$^{nu/nu}$ mice.

Results. ALCAM expression was significantly upregulated in NSCLC brain metastasis (p=0.023) with a *de novo* expression of ALCAM in 31.2% of brain metastases. Moderate/strong ALCAM expression in both primary NSCLC and brain metastasis was associated with shortened survival. Functional analysis of ALCAM knock-out (KO) cell line showed a significantly decreased cell adhesion capacity to human brain endothelial cells by 38% (p=0.045). *In vivo* studies showed significantly lower tumor cell dissemination in mice injected with ALCAM-KO cells in both mouse models and both the number and size of brain metastases were significantly diminished in ALCAM depleted tumors.

Conclusions. Our findings suggest that elevated levels of ALCAM expression promote brain metastases formation in NSCLC through increased tumor cell dissemination and interaction with the brain endothelial cells. Therefore, ALCAM could be targeted to reduce the occurrence of brain metastasis.

Keywords: ALCAM adhesion, NSCLC brain metastasis, blood-brain barrier

Key Points

- ALCAM expression associates with poor prognosis and brain metastasis in NSCLC.
- ALCAM mediates interaction of NSCLC tumor cells with brain vascular endothelium.
- ALCAM might represent a novel preventive target to reduce the occurrence of brain metastases in NSCLC.

Importance of the Study

Lung cancer patients with brain metastasis have a very poor prognosis. Recent studies have demonstrated the importance of cell adhesion molecules in the tumor cell dissemination and metastasis process. The brain is a unique site of metastasis since it is protected by the blood-brain barrier. We have identified the expression of cell adhesion molecule ALCAM to be upregulated in brain metastases of lung cancer patients which is furthermore associated with poor outcome. Importantly, our results indicate that ALCAM is directly involved in brain metastasis formation by promoting adherence to the cerebrovascular endothelium. As ALCAM inhibition is currently evaluated in an ongoing Phase II study for treatment of solid tumors, future evaluation of ALCAM expression may better stratify patients for

optimized treatment. Additionally, our study is the first showing that ALCAM contributes to brain metastasis formation in NSCLC and could be a potential therapeutic target.

2. Introduction

Lung cancer is the most common cause of cancer-related death, accounting for about 27% of all cancer deaths[1,2]. Despite new treatment, the five-year survival rate of non-small cell lung cancer (NSCLC) remains only around 15% in developed countries, with most cases being diagnosed in advanced stages with very poor outcome[3]. Brain metastases (BM) are a frequent complication in lung cancer patients presenting in approximately 40% of patients with advanced adenocarcinoma and 50% with small-cell lung cancer (SCLC)[4,5]. Around 10% of adenocarcinoma patients present with brain metastasis at the time of initial diagnosis[6] and in 50% the brain is the only site of tumor relapse (oligo-metastasis)[7]. Patients with brain metastases have a very poor prognosis with a 5-year survival rate of 2.9% and a high burden of neurological symptoms[8-10]. One of the main problems for treatment of brain metastasis is the blood-brain barrier (BBB). The endothelial cells (ECs) of the BBB are non-fenestrated and reinforced by the basal membrane and the end-feet of astrocytes, tightly regulating the movement of molecules, ions and cells across the BBB thus creating a substantial barrier for drug delivery to the central nervous system (CNS)[11,12].

In the context of the "seed and soil" hypothesis the successful colonization of brain metastatic cells depends on specific properties of tumor cells to both access and survive in the brain[13,14]. Circulating tumor cells (CTCs) are the seeds of metastases and detection of CTCs in NSCLC patients negatively correlates with clinical outcome[15]. Interestingly, we and others have shown that CTCs from brain metastatic patients commonly are EpCAM negative and thus display mesenchymal and stem cell traits[16,17]. CTCs from breast cancer patients with brain metastases were shown to commonly express CD44, a protein involved in cell-cell interactions and cell adhesion[16]. Different cell adhesion molecules (CAMs) have been shown to be involved in the process of metastasis. A deregulation of CAMs contributes to the detachment of cells from the primary mass leading to tumor progression and to metastasis to distant sites[18,19]. In breast cancer brain metastasis, L1CAM has been shown to mediate the vascular cooption of tumor cells to brain-related microvascular endothelium, thereby promoting brain metastasis formation[20,21]. Other CAMs have also been implicated to play an important role in brain metastases formation of different tumor entities[22] including activated leukocyte cell adhesion molecule

(ALCAM) in early stages of breast cancer metastasis seeding to the brain and vascular CAM-1 (VCAM-1) promoting adhesion of prostate carcinoma cells to brain ECs[23,24].

In this study, we investigated the role of ALCAM in NSCLC brain metastasis formation. Both primary NSCLC tumor tissue as well as brain metastatic tissue were investigated. ALCAM expression was found to be significantly associated with brain metastases and thus its functional role was investigated in both *in vitro* and mouse models.

3. Materials & Methods

3.1 Patient materials

Tissue micro arrays (TMA) of formalin fixed, paraffin embedded (FFPE) tissues including tissue from 51 primary lung tumors, 15 lymph node metastases and 76 lung cancer brain metastases were examined. Additionally, whole sections of 16 matched pairs of primary lung tumor tissue and corresponding brain metastases were analyzed. Furthermore, serum ALCAM levels were measured in 120 NSCLC patients, including 62 early staged non-metastatic patients, 34 multi-metastatic patients and 24 oligo brain metastatic patients. All patients had undergone surgery of both primary tumor and brain metastases at the University Medical Center Hamburg-Eppendorf between 1998 –2015. Ethical approval for this study was granted by the IRB Ethical Review Board of Hamburg analyses of human materials (PV4954). See also Supplementary Material.

3.2 Immunohistochemistry

For immunohistochemistry, ALCAM antibody (1:400, Vector laboratories, VP-C375) was visualized by Dako REAL Detection System (Peroxidase/ DAB+, K5001) according to manufacturer's protocol and counterstained with haematoxylin. See also Supplementary Material.

3.3 Detection of circulating tumor cells (CTCs)

37 metastatic NSCLC patients were screened for CTCs using a microfluidic device (Parsortix, Angle plc)[25]. 7.5ml of peripheral blood was collected in EDTA-tubes and processed immediately by the Parsortix device, followed by a cytocentrifugation of the obtained cells onto slides. The cells were visualized by immunofluorescence staining using antibodies against human keratins (1:100, clone AE1/AE3, eBioscience), ALCAM (1:150, clone 3A6, Biolegend) and CD45 (1:150; clone HI30, Biolegend). CTCs were defined as keratin+/dapi+/CD45-. See also Supplementary Material.

3.4 ALCAM ELISA

A sandwich enzyme-linked immunosorbent-assay (ELISA) was used to quantify peripheral blood serum levels of sALCAM using the DuoSet ELISA Development kit (R&D Systems, DY656) according to the

manufacturer's protocol. The probes were analyzed in 96-well microtiter plates as duplicates using a microplate reader set to 450nm (*InfiniteM200Pro*, Tecan NanoQuant,).

3.5 Generation of ALCAM-knock out (KO) cell line

Human NCI-H460 (hereafter H460) were obtained from ATCC (Manassas, USA). CRISPR-Cas9 technology was used to establish ALCAM knock-out (KO) cells. Successful ALCAM-KO was verified by immunoblot analysis and Sanger sequencing of individual expanded cell clones. Finally, a pool of five individually expanded H460 ALCAM-KO cell clones was used for all further experiments. See also Supplementary Material.

3.6 Proliferation, Migration and Colony Formation

Cellular proliferation was assessed by MTT assay. For migration a Boyden-chamber assay was used and colony formation was evaluated in soft agar assays. Adhesion capacity on human ECs was evaluated by using a static adhesion test as well as under dynamic conditions. See also Supplementary Material.

3.7 Scanning electron microscopy

Parental and ALCAM-KO H460 cells were plated individually or as a mixture (1:1) with brain ECs (HBEC-5i) and grown on 0.5% gelatin-coated coverslips for 2 days. Thereafter, samples were fixed in 2% glutaraldehyde for 1h at RT and then overnight at 4°C. Following a 16h post-fixation in 1% OsO_4 at 4°C, they were dehydrated in an acetone gradient (25–100%) and critical point dried in a CO_2 system (Critical Point Dryer, Leica Microsystems, EM CPD 300). Samples were then sputter coated with gold (sputter coating device SCD 050, BAL-TEC GmbH) and examined at a 5-kV accelerating voltage in field emission-scanning electron microscope (Jeol JSM 7500F).

3.8 Animal experiments

All mice experiments were performed in accordance with the guidelines of animal welfare of the University Medical Center Hamburg-Eppendorf and the local authorities (Behörde für Soziales, Gesundheit und Verbraucherschutz Hamburg, Germany). Mice were kept on a 12:12 light-to-dark cycle with *ad libitum* access to food and water.

Two different mouse models were used. Parental and ALCAM-KO H460 cells were injected either intracranially in the right striatum (n=5 per group) or intracardially into the left ventricle (n=10 per group) of 12 week-old female NMRI-*Foxn1*$^{nu/nu}$ mice, respectively. Based on pilot experiments, mice were sacrificed 10 days after intracranial injection or by reaching a weight loss of more than 10% after intracardial injection (between days 17 to 21). One mouse injected intracranially with H460 ALCAM-KO cells did not show any signs of a brain tumor, most likely due to a faulty injection and was thus excluded from further analysis. Similarly, in the intracardial injection model one mouse in each group was excluded due to probably failed injection and therefore no tumor formation. Blood was collected from the eye vein, bone marrow was isolated from the left femur and tibia, whole brain and peripheral organs were paraffin-embedded. Brain tumor growth was calculated as $V_t = (\sqrt{(max.cross-sectional\ area)})^3$ as described in Kunkel et al.[26]. The metastases in the ventricles in the intracranial model were not considered for tumor volume calculation. CD34 positive blood vessels were counted as described in Kunkel et al.[26]. In brief, blood vessels per cross sectional area were counted in 10 hpfs for intracranial injected tumors. As brain tumors induced through intracardial injection were smaller in size, blood vessels per total cross sectional area were counted. Liquid biopsy analysis for CTC and DTC number in mouse blood and bone marrow was performed and visualized by immunofluorescence staining for human pan-keratin (1:100, clone AE1/AE3, eBioscience) and mouse CD45 (1:150, clone 30-F11, BD Pharmingen). For automatic cell identification the *Xcyto® Quantitative Cell Imager* (Chemometec, Denmark) was used[27]. Histology and µCT analysis of the spines and the right femora were performed as described in Supplementary Material.

3.9 Statistics

Data are presented as group averages ± standard deviation (s.d.) or median ± intraquartile range. Statistical analysis of patient samples was performed using SPSS 23.0. The correlation of clinical and pathological variables with the staining was examined using the Chi-square-test (x^2 – test) or Fisher's exact test. Kaplan-Meier survival curves were compared with the log-rank test. Statistical analysis of mice samples was performed using Graph Pad Prism 8.0. For simple comparison student's t-test or Mann-Whitney test was performed. A $p < 0.05$ was accepted as significant.

Further information is provided in Supplementary Material.

4. Results

4.1 ALCAM protein expression in NSCLC primary tumors and metastases

Immunohistochemical staining was performed for ALCAM on TMAs. ALCAM protein expression data was obtained from 47 primary tumors (PT), 15 lymph node metastases and 71 brain metastasis samples. ALCAM expression was significantly increased in brain metastases compared to primary tumor tissue (Figure 1A-D, p=0.023) as well as in lymph node metastases compared to primary tumor tissue (p=0.041). 50.7% of brain metastases showed a strong ALCAM expression compared to 46.6% of lymph node metastases and 27.7% of primary tumors. In order to evaluate the change in ALCAM expression from the primary tumor tissue to the brain metastatic tissue, 16 whole sections of matched pairs were analyzed. 37.5% (n=6) of the primary tumors showed no ALCAM expression, whereas only one specimen of the matched brain metastasis was negative for ALCAM, indicating a *de novo* expression of ALCAM in 31.2% of brain metastases. In one patient, two brain metastases diagnosed and operated one year apart showed very strong ALCAM expression in comparison to the negative primary tumor tissue (Figure 1A-C). Additionally, 25% (n=4) of samples showed an increase from moderate to strong ALCAM expression.

4.2 ALCAM expression in correlation with clinicopathological parameters and prognosis

Correlation between the ALCAM protein expression pattern and clinicopathological parameters was assessed. A strong ALCAM expression in primary NSCLC tumors was only significantly correlated with a positive lymph node status (p=0.019) (Table 1), whereas in brain metastatic tissue we found ALCAM to be correlated with both an oligo brain metastatic status (brain as only site of metastasis, p=0.046) as well as the presence of brain metastases at initial diagnosis (p=0.034). Survival analysis showed a correlation between ALCAM expression and overall survival (OS) in both primary tumors as well as brain metastases samples. Patients with strong ALCAM expression in their primary tumors showed a significantly shortened OS compared to tumors with less ALCAM expression (Figure 1E,

p=0.017). Likewise, a strong or moderate ALCAM expression in brain metastases correlated with a shorter brain specific OS (Figure 1F, p=0.035).

4.3 ALCAM expression on Circulating Tumor Cells (CTCs) and matched brain metastases

As we detected a *de novo* expression of ALCAM in a substantial number of brain metastases, we investigated whether this *de novo* expression occurred during dissemination or rather during outgrowth of the metastasis in the brain. To this end, we analyzed the ALCAM expression on CTCs isolated by Parsortix (Figure 2A) and matched brain metastases (Figure 2B). Keratin positive CTCs were found in 4 out of 37 NSCLC patients with brain metastases. In all these patients, we found congruent expression patterns of ALCAM on both CTCs and the matched brain metastasis tissue (Figure 2C). Sadly no matching primary tumors tissue was available for these patients.

4.4 sALCAM in plasma levels of NSCLC patients

ALCAM exists both as a transmembrane as well as a secreted protein (sALCAM)[28]. To analyze if also the secreted sALCAM is associated with brain metastasis, sALCAM was quantified in peripheral blood plasma samples using a sandwich enzyme-linked immunosorbent-assay (ELISA). 120 NSCLC patients with early-staged (n=62), advanced multi metastatic (n=34) or oligo-brain metastatic (n=24) disease were analyzed. sALCAM levels were significantly elevated in the serum of multi- metastatic NSCLC patients (Figure 2D, n=34; mean 2338 pg/ml) compared to non-metastatic patients (n=62; mean 1772 pg/ml; p=0.001). The sALCAM serum levels of multi-metastatic NSCLC patients were also significantly elevated compared to oligo-brain metastatic patients (n=24; mean 1700 pg/ml; p=0.02). We defined the median sALCAM value as cut-off value for the categorical analysis of sALCAM data in association with histopathological data. An elevated sALCAM level showed neither a significant correlation with any histopathological data nor with patient survival indicating that the cellular ALCAM is more important for brain metastasis formation than the soluble form.

4.5 *In vitro* model of ALCAM function in NSCLC

To elucidate a role of ALCAM in the formation of brain metastasis in lung cancer, we established an *in vitro* model by using the NSCLC cell line NCI-H460. This cell line, derived from a pleural effusion of

a NSCLC patient, has been shown to be able to metastasize to the brain and other organs[21]. Using the CRISPR/Cas9 technology, a targeting plasmid for ALCAM inactivation was introduced in these cells and ALCAM absence was confirmed after cell expansion by immunoblot and immunofluorescence labeling (Figure 3A, Suppl. Figure 1A, B). Assays were performed to test whether the absence of ALCAM influenced basic cell functions. We observed no effect on proliferation (Figure 3B), migration (Figure 3C) and colony formation (Figure 3D).

As ALCAM is an adhesion molecule, the effect of ALCAM inactivation on adhesion on different surfaces was assessed. A static adhesion assay in co-culture with brain ECs (hCMEC/D3) was performed. GFP-fluorescence intensity was measured after washing using *infiniteM200* (Tecan). The adhesion of H460 ALCAM-KO cells to brain ECs was significantly decreased by 29% ($p \leq 0.001$) compared to H460 parental cells (Figure 3E). To further assess this interaction, adhesion under flow conditions, mimicking the blood stream in microvessels, was performed[29]. Adhesion of both parental and ALCAM-KO H460 cells is impaired under shear stress, however to different extent: 38% of H460 ALCAM-KO cells compared to 19% of H460 parental cells ($p=0.045$) detached from the EC monolayer under shear stress (Figure 3F) indicating that ALCAM plays a role in cell adhesion to brain ECs.

As the adhesion of ALCAM-KO cells on brain ECs was significantly decreased, we assessed the interaction more closely using scanning electron microscope (SEM). When the cells were grown on gelatin, the H460 parental cells showed a more flattened shape and had numerous cell ruffles on the cell surface (Figure 3G, H). In contrast, the ALCAM-KO cells showed a rounder shape possibly indicating a lower attachment to the surface. Interestingly, the ALCAM-KO cells did not have many ruffles on the surface but instead displayed more microvilli (Figure 3J, K). When grown together with human brain ECs, both the parental and ALCAM-KO cells interacted with the ECs. However, the contact was much more pronounced in the parental cells (Figure 3M) compared to a contact via the microvilli in the ALCAM-KO cells (Figure 3N). Immunofluorescence staining of CD9, a known interaction partner of ALCAM[30,31], revealed localization to the membrane ruffles in parental cells whereas it re-localized in microvillar-like structures in ALCAM KO cells (Suppl. Figure 1C-F).

4.5 *In vivo* ALCAM model

We injected the parental and ALCAM-KO H460 cells either intracranially or intracardially in nude mice to determine if inactivation of ALCAM affected tumor outgrowth in the brain or dissemination. In the intracranial model, at time of sacrifice large tumors were detected in the brain but no overt tumors (serial sectioning) were seen outside the brain. However, a significant difference in the number of CTCs was detected. 29 CTCs per 1 million blood cells (PBMCs) were found in mice injected with H460 parental cells, whereas no CTCs were found in the H460 ALCAM-KO injected mice (Figure 4B). Similarly, analysis for DTCs in the bone marrow revealed 44% fewer DTCs (20 DTCs / 1 million PBMCs) in H460 ALCAM-KO injected mice compared to H460 parental injected ones (36 DTCs / 1 million PBMCs) (Figure 4E). Although the median size of brain tumors was lower in H460 ALCAM-KO injected animals, the difference did not reach significance (Figure 5A, B, D; parental 140.1, range 80.2 - 237.1 mm^3, ALCAM-KO 67, range 28.7 – 160.4 mm^3, p=0.1905). Interestingly, a tumor growth could be found in the lateral ventricles of all mice injected with ALCAM-KO H460 cells, which was not observed in any of the parental H460 injected animals (Figure 5C, 0/5). Due to the location of the injection site (tracking of needle path), we believe that the cells were not injected in the ventricle rather that the cells migrated there. To analyze whether the induced tumors are differentially vascularized, immunohistochemical staining for the endothelial cell adhesion molecule CD34 was performed with no difference observed between the two groups in terms of number, size or form of vessels (Suppl. Figure 2A-C). Finally, as bone is the most common site of metastases in cancer patients, we searched bone remodeling in the vertebral bodies and femur by sections and µCT respectively. No signs of osteolytic lesions or bone remodeling, neither in spine, nor in femora assessed by µCT was observed (Suppl. Figure 2E, F, I-L).

To assess the involvement of ALCAM in the dissemination to the brain, we performed intracardiac injection of parental und ALCAM-KO H460 cells. At time of sacrifice, mice injected with H460 parental cells had significantly more brain metastases compared to ALCAM-KO injected mice (Figure 5E, F, G; parental 24, range 16–45 ALCAM-KO 14 range 1-18, p=0.0004) and showed a significantly higher total tumor load throughout the brain (Figure 5H; parental 8.93, range 1.3-23.2 mm^3, ALCAM-KO 2.08, range 0.1-7.6 mm^3, p=0.0078). None of the mice showed signs of metastasis in the ventricles. No

differences in the form and number of blood vessels were found (Suppl. Figure 2D). Similarly to the intracranial model, CTC analysis revealed 68% less CTCs per 1 million PBMCs in mice injected with H460 ALCAM-KO cells compared to H460 parental injected ones (parental 85 CTCs / 1 million PBMCs, ALCAM-KO 27 CTCs / 1 million PBMCs; Figure 4C). Analysis of undecalcified vertebral body sections revealed metastases in the spine and femur of both groups, which was independent of ALCAM (Suppl. Figure 2G, H M-P). However, we could observe a decrease in bone mineral density of the femora in H460 parental injected mice (Suppl. Figure 2Q, parental 793.3 ± 25.9, ALCAM-KO 828.4 ± 12.7).

5. Discussion

Cell adhesion is essential for cell communication and cell architecture. In tumor progression a change of cell architecture contributes to dissemination and metastasis[18,32]. ALCAM has previously been shown to be involved in tumor progression and metastasis[18,33-35] but the potential impact of this protein on brain metastasis formation is currently unknown. In this study we analyzed the protein expression of ALCAM in primary tumors, CTCs and brain metastases and assessed its functional role in tumor dissemination, adhesion and brain metastasis formation in *in vitro* and *in vivo* models.

In our analysis, ALCAM expression was found to be significantly elevated in brain metastases compared to primary tumors. Specifically, in matched tissue an ALCAM upregulation from the primary tumors to brain metastases in one third of cases was found, suggesting an important role in brain metastasis. Positive ALCAM status in primary NSCLC tumors has previously been linked to poor prognosis[31]. Here we show that it is particularly connected to NSCLC brain metastasis but also lymph node metastasis. Importantly, an elevated level of ALCAM expression in both the primary tissue and brain metastases was associated with a shorter overall survival (both $p<0.05$). In order to assess at which stage ALCAM upregulation might take place, matched CTCs and brain metastases were analyzed for ALCAM expression. Although of clinical relevance, CTCs are rare in oligo-brain metastatic NSCLC[36] and therefore the ALCAM expression could be assessed in CTCs from only four patients. CTCs and brain metastasis samples showed in all cases a congruent ALCAM expression, suggesting that ALCAM expression of CTCs in the peripheral blood might represent the ALCAM status of the brain metastasis.

However, further studies would need to be performed especially on patients before they develop overt brain metastasis detectable by imaging in order to assess the CTCs with “true brain metastasis seed”.

We further analyzed whether the soluble sALCAM form in blood serum could serve as an additional non-invasive biomarker. sALCAM is formed through shedding of its ectodomain by the metalloprotease ADAM17/TACE[28] and high levels have been associated with a more aggressive tumor type in epithelial ovarian cancer[36]. We found sALCAM serum levels significantly elevated in multi-metastatic NSCLC patients compared to non-metastatic tumor patients and oligo-brain-metastatic patients. As in other tumor entities sALCAM might function as a general marker for dynamic tumor progression, in NSCLC it can be discussed as an overall prognostic factor not specifically linked to brain metastasis[36-38].

Based on these observations we assumed that ALCAM expression might in particular affect brain metastasis formation of NSCLC cells. Hence we sought to test our hypothesis in an ALCAM-depleted NSCLC cell line model. ALCAM is known to promote cell migration associated with tumor progression and metastasis in other tumor entities[34,39-42]. Importantly, ALCAM has been shown to be crucial for leucocyte transendothelial migration through the BBB[43-45]. Our functional analysis of H460 ALCAM-depleted cells showed no changes in cell viability but a significant decrease in cell adhesion. By using both, a static assay and under flow condition mimicking the blood stream in microvessels, we showed that the adhesion capacity of ALCAM-depleted cells to brain endothelial cells was significantly reduced. This effect is similar to L1CAM, which promotes breast cancer brain metastasis formation by vascular co-option of brain vascular endothelium [20]. We assume that ALCAM might be important for facilitating the extravasation of lung tumor cells through the BBB by mediating adhesion by both heterophilic (ALCAM-CD9) and homophilic (ALCAM-ALCAM) cell adhesion[30,46]. Brain ECs express high levels of ALCAM[43] facilitating a strong cell contact between tumor cells expressing ALCAM and ECs. Further assessment using scanning electron microscope showed an altered shape of ALCAM-depleted cells indicating a cell architecture disruption and adhesion deficiency both at the apical (ruffles versus microvilli) and lateral (cell shape) sides of the cells. Although both cells (parental and ALCAM-KO) seem to interact with the brain ECs, a stronger contact is mediated through the ruffles in the parental cells, whereas ALCAM-KO cells were less strongly connected to the ECs via the microvilli.

Interestingly, silencing ALCAM promoted an upregulation of its interacting partner CD9 that transforms the cellular morphology and eventually their migration. This hypothesis is supported by the study of Rappa et al., who showed that the knockdown of CD9 in breast cancer cells promoted the formation of membrane ruffles instead microvilli[47].

In order to assess if ALCAM is involved in both the tumor cell dissemination across the BBB, as well as outgrowth in the brain, we used two different *in vivo* mouse models. We could show that intracardially injected H460 ALCAM-KO cells lead to fewer brain metastases with less total tumor load compared to the parental cell line. In contrast, tumor outgrowth was unaffected by the ALCAM status in the intracranial model. This data supports our hypothesis that ALCAM is rather involved in tumor dissemination than metastatic outgrowth. Moreover, in the intracranial model no CTCs could be detected in the mice injected with ALCAM-KO cells. Similarly, also the intracardial injection model showed a significant decrease (68%) in CTCs when ALCAM-KO cells were injected compared to parental cells. It has been shown that CTCs from primary brain tumors can exit the brain to the circulation[48,49]. This indicates that the BBB is not an unpassable barrier for CTCs. Accordingly, we identified less CTCs in the intracranial model of parental H460 ALCAM cells compared to the cardiac injection. The lack of CTCs in the intracranial ALCAM-KO model could indicate a problem in passing the BBB due to impaired adhesion of the tumor cells to brain endothelial cells, as shown by our *in vitro* data. However, the intracardiac model indicates that ALCAM might also give the tumor cells a survival advantage in the blood circulation. Thus, ALCAM might be involved in metastasis formation through different mechanisms.

We couldn't find any differences in either the vessel counts between the models indicating no significant impact of ALCAM on angiogenesis nor in the formation of bone metastases. Obviously, this data of ALCAM associated differential dissemination and metastatic patterns needs to be verified using different models prospectively.

In summary, we demonstrated elevated ALCAM expression levels in human NSCLC brain metastases. We showed that an ALCAM-positive status is correlated with poor outcome in lung cancer patients in

both primary tumor setting as well as among brain metastatic patients. Further *in vitro* and *in vivo* findings support a role for ALCAM in brain dissemination and outgrowth, most likely via the interaction with brain ECs. Currently the first phase II trial is ongoing in which an ALCAM-directed probody drug conjugate is being tested on different primary cancer entities[50]. This emphasizes the potential clinical use of ALCAM as a novel therapeutic target. Our results suggest that in addition ALCAM might also represents a novel preventive target to reduce the occurrence of brain metastases in NSCLC.

Acknowledgments

The authors would like to thank Jolanthe Kropidlowski, Svenja Zapf and Michael Horn-Glander for technical assistance.

References

1. Torre LA, Bray F, Siegel RL, Ferlay J, Lortet-Tieulent J, Jemal A. Global cancer statistics, 2012. *CA Cancer J Clin.* 2015; 65(2):87-108.
2. Malvezzi M, Bertuccio P, Rosso T, et al. European cancer mortality predictions for the year 2015: does lung cancer have the highest death rate in EU women? *Ann Oncol.* 2015; 26(4):779-786.
3. Torre LA, Siegel RL, Jemal A. Lung Cancer Statistics. *Adv Exp Med Biol.* 2016; 893:1-19.
4. Dawe DE, Greenspoon JN, Ellis PM. Brain metastases in non-small-cell lung cancer. *Clin Lung Cancer.* 2014; 15(4):249-257.
5. Lassen U, Kristjansen PE, Hansen HH. Brain metastases in small-cell lung cancer. *Ann Oncol.* 1995; 6(9):941-944.
6. Villano JL, Durbin EB, Normandeau C, Thakkar JP, Moirangthem V, Davis FG. Incidence of brain metastasis at initial presentation of lung cancer. *Neuro Oncol.* 2015; 17(1):122-128.
7. Hu C, Chang EL, Hassenbusch SJ, 3rd, et al. Nonsmall cell lung cancer presenting with synchronous solitary brain metastasis. *Cancer.* 2006; 106(9):1998-2004.
8. Hall W, Djalilian H, Nussbaum E, Cho K. Long-term survival with metastatic cancer to the brain. *Medical Oncology.* 2000; 17(4):279-286.
9. Ali A, Goffin JR, Arnold A, Ellis PM. Survival of patients with non-small-cell lung cancer after a diagnosis of brain metastases. *Curr Oncol.* 2013; 20(4):e300-306.
10. Chamberlain MC, Baik CS, Gadi VK, Bhatia S, Chow LQ. Systemic therapy of brain metastases: non-small cell lung cancer, breast cancer, and melanoma. *Neuro Oncol.* 2017; 19(1):i1-i24.
11. Zlokovic BV. The blood-brain barrier in health and chronic neurodegenerative disorders. *Neuron.* 2008; 57(2):178-201.
12. Daneman R. The blood-brain barrier in health and disease. *Ann Neurol.* 2012; 72(5):648-672.
13. Ramakrishna R, Rostomily R. Seed, soil, and beyond: The basic biology of brain metastasis. *Surg Neurol Int.* 2013; 4(Suppl 4):S256-264.
14. Witzel I, Oliveira-Ferrer L, Pantel K, Muller V, Wikman H. Breast cancer brain metastases: biology and new clinical perspectives. *Breast Cancer Res.* 2016; 18(1):8.

15. Hanssen A, Wagner J, Gorges TM, et al. Characterization of different CTC subpopulations in non-small cell lung cancer. *Sci Rep.* 2016; 6:28010.

16. Boral D, Vishnoi M, Liu HN, et al. Molecular characterization of breast cancer CTCs associated with brain metastasis. *Nat Commun.* 2017; 8(1):196.

17. Hanssen A, Loges S, Pantel K, Wikman H. Detection of Circulating Tumor Cells in Non-Small Cell Lung Cancer. *Front Oncol.* 2015; 5:207.

18. Wai Wong C, Dye DE, Coombe DR. The role of immunoglobulin superfamily cell adhesion molecules in cancer metastasis. *Int J Cell Biol.* 2012; 2012:340296.

19. Beauchemin N, Arabzadeh A. Carcinoembryonic antigen-related cell adhesion molecules (CEACAMs) in cancer progression and metastasis. *Cancer Metastasis Rev.* 2013; 32(3-4):643-671.

20. Valiente M, Obenauf AC, Jin X, et al. Serpins promote cancer cell survival and vascular co-option in brain metastasis. *Cell.* 2014; 156(5):1002-1016.

21. Kienast Y, von Baumgarten L, Fuhrmann M, et al. Real-time imaging reveals the single steps of brain metastasis formation. *Nat Med.* 2010; 16(1):116-122.

22. Wilhelm I, Molnar J, Fazakas C, Hasko J, Krizbai IA. Role of the blood-brain barrier in the formation of brain metastases. *Int J Mol Sci.* 2013; 14(1):1383-1411.

23. Brayton J, Qing Z, Hart MN, VanGilder JC, Fabry Z. Influence of adhesion molecule expression by human brain microvessel endothelium on cancer cell adhesion. *J Neuroimmunol.* 1998; 89(1-2):104-112.

24. Soto MS, Serres S, Anthony DC, Sibson NR. Functional role of endothelial adhesion molecules in the early stages of brain metastasis. *Neuro Oncol.* 2014; 16(4):540-551.

25. Hvichia GE, Parveen Z, Wagner C, et al. A novel microfluidic platform for size and deformability based separation and the subsequent molecular characterization of viable circulating tumor cells. *Int J Cancer.* 2016; 138(12):2894-2904.

26. Kunkel P, Ulbricht U, Bohlen P, et al. Inhibition of glioma angiogenesis and growth in vivo by systemic treatment with a monoclonal antibody against vascular endothelial growth factor receptor-2. *Cancer Res.* 2001; 61(18):6624-6628.

27. Koch C, Joosse SA, Schneegans S, et al. Pre-analytical and analytical variables of label-independent enrichment and automated detection of circulating tumor cells in cancer patients (submitted).

28. Rosso O, Piazza T, Bongarzone I, et al. The ALCAM shedding by the metalloprotease ADAM17/TACE is involved in motility of ovarian carcinoma cells. *Mol Cancer Res.* 2007; 5(12):1246-1253.

29. Kalagara T, Moutsis T, Yang Y, et al. The endothelial glycocalyx anchors von Willebrand factor fibers to the vascular endothelium. *Blood Adv.* 2018; 2(18):2347-2357.

30. Gilsanz A, Sanchez-Martin L, Gutierrez-Lopez MD, et al. ALCAM/CD166 adhesive function is regulated by the tetraspanin CD9. *Cell Mol Life Sci.* 2013; 70(3):475-493.

31. von Lersner A, Droesen L, Zijlstra A. Modulation of cell adhesion and migration through regulation of the immunoglobulin superfamily member ALCAM/CD166. *Clin Exp Metastasis.* 2019; 36(2):87-95.

32. Raz A, Ben-Ze'ev A. Cell-contact and -architecture of malignant cells and their relationship to metastasis. *Cancer Metastasis Rev.* 1987; 6(1):3-21.

33. Ishiguro F, Murakami H, Mizuno T, et al. Membranous expression of activated leukocyte cell adhesion molecule contributes to poor prognosis and malignant phenotypes of non-small-cell lung cancer. *J Surg Res.* 2013; 179(1):24-32.

34. Devis L, Moiola CP, Masia N, et al. Activated leukocyte cell adhesion molecule (ALCAM) is a marker of recurrence and promotes cell migration, invasion, and metastasis in early-stage endometrioid endometrial cancer. *J Pathol.* 2017; 241(4):475-487.

35. Ofori-Acquah SF, King JA. Activated leukocyte cell adhesion molecule: a new paradox in cancer. *Transl Res.* 2008; 151(3):122-128.

36. Carbotti G, Orengo AM, Mezzanzanica D, et al. Activated leukocyte cell adhesion molecule soluble form: a potential biomarker of epithelial ovarian cancer is increased in type II tumors. *Int J Cancer.* 2013; 132(11):2597-2605.

37. Tachezy M, Effenberger K, Zander H, et al. ALCAM (CD166) expression and serum levels are markers for poor survival of esophageal cancer patients. *Int J Cancer.* 2012; 131(2):396-405.

38. Arnold Egloff SA, Du L, Loomans HA, et al. Shed urinary ALCAM is an independent prognostic biomarker of three-year overall survival after cystectomy in patients with bladder cancer. *Oncotarget.* 2017; 8(1):722-741.

39. Weidle UH, Eggle D, Klostermann S, Swart GW. ALCAM/CD166: cancer-related issues. *Cancer Genomics Proteomics.* 2010; 7(5):231-243.

40. Ishiguro F, Murakami H, Mizuno T, et al. Activated leukocyte cell-adhesion molecule (ALCAM) promotes malignant phenotypes of malignant mesothelioma. *J Thorac Oncol.* 2012; 7(5):890-899.

41. Lunter PC, van Kilsdonk JW, van Beek H, et al. Activated leukocyte cell adhesion molecule (ALCAM/CD166/MEMD), a novel actor in invasive growth, controls matrix metalloproteinase activity. *Cancer Res.* 2005; 65(19):8801-8808.

42. Degen WG, van Kempen LC, Gijzen EG, et al. MEMD, a new cell adhesion molecule in metastasizing human melanoma cell lines, is identical to ALCAM (activated leukocyte cell adhesion molecule). *Am J Pathol.* 1998; 152(3):805-813.

43. Cayrol R, Wosik K, Berard JL, et al. Activated leukocyte cell adhesion molecule promotes leukocyte trafficking into the central nervous system. *Nat Immunol.* 2008; 9(2):137-145.

44. Masedunskas A, King JA, Tan F, et al. Activated leukocyte cell adhesion molecule is a component of the endothelial junction involved in transendothelial monocyte migration. *FEBS Lett.* 2006; 580(11):2637-2645.

45. Bowen MA, Patel DD, Li X, et al. Cloning, mapping, and characterization of activated leukocyte-cell adhesion molecule (ALCAM), a CD6 ligand. *J Exp Med.* 1995; 181(6):2213-2220.

46. van Kempen LC, Nelissen JM, Degen WG, et al. Molecular basis for the homophilic activated leukocyte cell adhesion molecule (ALCAM)-ALCAM interaction. *J Biol Chem.* 2001; 276(28):25783-25790.

47. Rappa G, Green TM, Karbanova J, Corbeil D, Lorico A. Tetraspanin CD9 determines invasiveness and tumorigenicity of human breast cancer cells. *Oncotarget.* 2015; 6(10):7970-7991.

48. Muller C, Holtschmidt J, Auer M, et al. Hematogenous dissemination of glioblastoma multiforme. *Sci Transl Med.* 2014; 6(247):247ra101.

49. Sullivan JP, Nahed BV, Madden MW, et al. Brain tumor cells in circulation are enriched for mesenchymal gene expression. *Cancer Discov.* 2014; 4(11):1299-1309.

50. ClinicalTrials.gov. PROCLAIM-CX-2009: A Trial to Find Safe and Active Doses of an Investigational Drug CX-2009 for Patients With Selected Solid Tumors. 2017; NCT03149549. Available at: https://clinicaltrials.gov/ct2/show/study/NCT03149549?term=CD166&rank=4. Accessed July 19, 2019.

Figure 1. ALCAM expression in primary tumor and metastatic tissue from NSCLC patients. ALCAM protein expression in (A) primary tumor (PT) and (B, C) two different brain metastases (BM) from a NSCLC patient. (D) Frequency of ALCAM expression in PT, lymph node metastases (LN) and BM tissue (PT – BM p=0.023, PT – LN p=0.04). Survival analysis by Kaplan-Meier showing a significant shortened overall survival for patients with positive ALCAM protein expression in (E, strong n=13, other n=33) NSCLC primary tumors and (F, moderate n=9, strong n=16, negative n=5)) NSCLC brain metastases. The p-value was determined using the log-rank test. Scale bar 20µm.

Figure 2. ALCAM as brain metastasis marker in liquid biopsy. Immunofluorescent staining of ALCAM on a (A) CTC and matched (B) brain metastasis sample. (C) Correlation of ALCAM expression on CTCs with matched NSCLC brain metastasis tissue. (D) sALCAM serum analysis in non-metastatic (M0), oligo-brain metastatic and multi-site-metastatic NSCLC patients showing significantly elevated sALCAM level in advanced cancer patients compared to early staged patients (p=0.001) and oligo-brain metastatic patients (p=0.02). Mean ± s.d. Scale bar 20µm.

Figure 3. Functional analyses of ALCAM in NSCLC cells. (A) Silencing of ALCAM in NCI-H460 cells by CRISPR/Cas ALCAM-KO was confirmed by immunoblot. Absence of ALCAM has no influence on proliferation (B, p=0.689), migration (C, p=0.895) and colony formation capacity (D, p=0.771). Adhesion on hCMEC/D3 EC under static conditions was significantly reduced in H460 ALCAM-KO cells compared to parental cells (E, p≤0.001). (F) Adhesion after exposure to shear stress was significantly reduced in ALCAM-KO cells (p=0.045). (G-N) Parental cancer H460 cells (G-I, M) and ALCAM KO counterparts (J-L, N) were cultured alone (G-L) or mixed (1:1) with EC (M, N), cultured for 2 days on gelatin-coated coverslips prior processing for scanning electron microcopy. Insets show higher magnification of certain regions indicated with boxes (M, N). Drawings show the appearance of plasma membrane protrusions at their surface (H, K). Asterisk, cancer cells; arrow, EC; m, magnupod. Mean ± s.d. Scale bars, 1 µm (H, K); 10 µm (G, I, J, L-N).

Figure 4. Liquid biopsy and tumor outgrowth in intracranial and intracardial injected mice. (A-C) Liquid biopsy from injected mice showing no detectable CTCs in the blood of intracranial injected mice (B) and less CTCs in the blood of intracardial injected mice (C) when H460 ALCAM-KO cells were injected. Analysis of bone marrow aspirates show less DTCs of H460 ALCAM-KO intracranial injected mice (E). Scale bars in A, D: 20µm

Figure 5. (A, B, D) Tumor outgrowth was not significantly different between parental (A) and ALCAM-KO (B) intracranial injected mice (D, p=0.1905). Tumor cells were detected in the lateral ventricle of ALCAM-KO intracranial injected mice (C, 4/4 injected mice), whereas in 0/5 of parental injected mice. (E, F). Representative pictures of whole brain sections from mice injected intracardially with either H460 parental (E) or H460 ALCAM-KO (F) cells showing number and size of tumors. Tumor number (G; p=0.0004) and total tumor volume (H, p=0.0078) is significantly higher in H460 parental injected mice. Median ± interquartile range. Scale bars in A-C: 500µm; in E, F: 1000µm, in inserts of E, F: 100µm.

Supplementary Material

1.1 Patient materials

Patient data were collected on sex, histological findings, tumor status (T), lymph node metastasis (N), metastases (M), disease stage (UICC). Clinical follow up (FUP) data were available from 46 primary NSCLC patients and 30 brain metastatic patients. The median follow-up time of the patients included in the survival analysis of the primary tumor cohort was 26.1 months (range 0.6 – 110.7 months) vs. 8.1 months (range 0.4 – 78.1 months) in the brain metastatic cohort. Overall survival (OS) was calculated from the initial diagnosis of the primary tumor or if applicable brain metastasis to death.

1.2 Immunochistochemistry

The specificity, optimal dilution and pre-treatment for ALCAM antibody was defined by testing well characterized positive (H1395) and negative (HTB56) cell lines, which were formalin fixed and paraffin embedded (FFPE). FFPE tissue was baked for 2 hours, dewaxed with xylene and gradually hydrated with alcohol. The slides were boiled in Antigen Retrival Citra Plus Solution (Biogenex, HK080-9K) for 5 minutes. After cooling down for 30 minutes the primary antibody (ALCAM 1:400, Vector laboratories, VP-C375) was incubated overnight at 4°C. The immunostaining was evaluated independently by two observers using a score including staining intensity and percentage of positive cells. The staining intensity was graded between 0 (none) and 3 (strong staining). Additionally, the percentage of positive cells was graded between 0 and 3, too (none= 0, <20% = 1, 20% - 69% = 2, ≥ 70% = 3). Final ALCAM scoring: score 0 was considered as negative, score <3.5 was considered as weak, score ≥ 3.5 <5 as intermediate and score ≥5 as strong expression.

1.3 Immunofluoresence of CTCs

For immunofluorescent staining cells were fixed for 10 min with 4% paraformaldehyde (PFA) at room temperature (RT). Cells were permeabilized for 10 minutes with 0.2% Triton X-100, blocked for 20 min with 10% AB-serum (BIO-RAD, 805135) and primary antibodies against ALCAM (1:50, 3A6,

Biolegend, 343902), pan-keratin antibody (1:80, AE1/AE3, eBioScience, 53-9003-82) and CD45 antibody (1:150, HI30, BioLegend, 304012) in 10% AB-serum were applied overnight at 4°C. Next day, Alexa 555 rabbit anti-mouse secondary antibody (1:200, Life Technologies, A11059) was applied for 45 minutes at RT. Nuclei were stained with DAPI (1 µg/mL; Sigma-Aldrich). Staining was analyzed using a Zeiss Axioplan 2 (Carl Zeiss AG, Oberkochen, Germany).

1.4 Western Blot

Whole-cell extracts from cultured cells were prepared by direct lysis and sonication of cells in 2% SDS sample buffer containing phosphatase and protease inhibitors. Cell extracts were separated in denaturing 10% gels and blotted onto nitrocellulose membrane. Detection of proteins was performed by incubation with the following specific antibodies: ALCAM (1:400; NovoCastra, 6034968) and HSC70 (1:2000; Santa Cruz, sc-7298) or GAPDH (1:5000, Santa Cruz, sc-25779). For detection HRP-secondary antibody (1:2000, Cell Signaling, 7076) was used.

1.5 Generation of ALCAM-knock out (KO) cell line

H460 Cells were grown in RPMI-1640 supplemented with fetal calf serum, L-Glutamin and penicillin/streptomycin. For creating ALCAM-KO H460 cells, human specific ALCAM CRISPR/Cas9 KO plasmids were purchased from Santa Cruz (sc-418418) and transfected with Lipofectamine 2000 (Invitrogen) into parental H460 cells, according to manufacturer's protocol. After 5 days, single GFP-positive cells were isolated using fluorescence activated cell sorting and clonally expanded. Stable GFP-expression was established using the LeGO-G2 plasmid according to standard protocol[1].

1.6 Proliferation, Migration and Colony Formation

Cellular proliferation was assessed by MTT assay. 1000 parental or ALCAM-KO H460 cells were seeded in quadruplicates in 96-well plates in RPMI. After 24 h, 72 h and 96 h 20 µl MTT was added per well and incubated for 3 h. Relative cell proliferation was estimated spectrophotometrically at E540nm (reference: E650nm) using *InfiniteM200Pro* and ratio of parental compared ALCAM-KO

H460 cells was calculated. For migration 5 x 10^3 parental or ALCAM-KO H460 cells were seeded in triplicates in a transwell inserts in 6-well plates with 8 µm pores size in serum-free RPMI. Number of migrated cells was estimated after 24 h by light microscopy of fixed cells stained with crystal violet. Colony formation was evaluated using soft agar assay. For this a bottom layer of 0.5 % agar with media was poured and solidified first, followed by an upper layer containing 2000 parental or ALCAM-KO H460 cells suspended in medium-agar mixture. After two weeks, the number of colonies was evaluated.

1.7 Static adhesion on brain endothelial cells

For assessing adhesion capacity on cerebral endothelial cells, 23 x 10^4 hCMEC/D3 cells were seeded in a 96-well plate per well, treated with 10 ng/ml TNF-α for 4 h before 5 x 10^4 parental or ALCAM-KO H460 cells were seeded on top. After 40 min cells were washed and cGFP-fluoresence intensity, resulting from the transduction plasmid, was measured using *InfiniteM200Pro*.

1.8 *In vitro* cell adhesion assay

A confluent monolayer of HMEC-5i (ATCC® CRL-3245™) cultured on a µ-Slide $I^{0.2}$ Luer IBIDI (IBIDI GmbH, Munich, Germany) was stimulated for 4 hours with 10 ng/ml of TNFα (PeproTech, Germany). 100 x 10^3 parental and 100 x 10^3 ALCAM-KO H460 cells were labeled with fluorescent Green and Orange AM Celltrace (1:1000; Invitrogen, Darmstadt, Germany), respectively. Later, cells were transferred together into 4 ml of equilibrated DMEM:F12 (ATCC® 302006™) and perfused over the HMEC-5i monolayer at 2.5 dyne/cm² by using an IBIDI pump system (IBIDI GmbH, Munich, Germany). After 1 minute of perfusion, flow was stopped and cell precipitation was allowed for 5 minutes. Upon cell deposition, randomly distributed pictures were taken for cell quantification. Then, flow was restarted and a second round of pictures was taken immediately at the same positions as before. Pictures were obtained using a Zeiss AxioObserver Z1 equipped with an AxioCam MRc (Carl Zeiss AG, Oberkochen, Germany). For quantification, cell number after cell deposition (set as 100%) and

within flow condition was counted. For assessing adherence capacity, we compared the latter cell number to the initial value.

As difference in adhesion the number of cells from the first pictures was set as 100% and difference in adhesion was calculated in comparison to 100%.

1.9 Indirect immunofluorescence labeling

Cell surface immunolabeling of parental and ALCAM-KO H460 cells growing for 2 days on 0.5% gelatin-coated coverslips was performed as described previously[2] using antibodies against either ALCAM (1:50, 3A6) or CD9 (1:50, M-L13, both BD Biosciences), visualized using Alexa 647 (or 488) goat-anti-mouse secondary antibody (Thermo Fisher Scientific) and the nuclei were stained with DAPI. Images were captured with Leica SP5 upright confocal microscope. Composites of 24 optical sections are shown. The images were prepared using Fiji and Adobe Illustrator software.

1.10 *In vivo* experiments

Mice were intracranial injected with a final concentration of 100 000 cells/µL in 0.9 % isotonic NaCl in 2 µL. Briefly, after anesthesia by injection of ketamine/xylazine, a small hole was drilled through the skull of the mouse and the cell solution was injected into the right striatum with a Hamilton syringe (needle gauge 30) at the following stereotactic coordinates from the bregma (0 mm, +2 mm, −2 mm).

In the intracardical model, after anesthesia with isoflurane, 10^6 cells in 100µl were injected in the left ventricle of the mouse heart by an experienced person. For better recovery, mice were allowed to wake up in an O_2 enriched chamber. All mice did not show any signs of illness after injection. For liquid biopsy analysis blood from 5 mice per group was pooled and CTCs were isolated using Ficoll density gradient centrifugation and spinned on slides. For DTC identification, bone marrow of the left femur and tibia was isolated by centrifugation of the bones and spinned on slides.

FFPE brain sections were stained with HE standard protocol to identify tumor size and outgrowth. For immunohistological staining antibodies against pan-cytokeratin (1:1000; AE1 MAB1612, AE3 MAB1611, both Millipore) and CD34 (1:125, abcam, ab8158) were used and detected by the Dako REAL Detection System (Peroxidase/ DAB+), as described above.

Skeletons were fixed in 3.7 % PFA for 24 h and subsequently stored in 80 % ethanol. For bone histology, the lumbar vertebral bodies L1 to L6 were dehydrated in ascending alcohol concentrations and embedded in methylmetacrylate as described previously[3]. Sections of 5 µm thickness were cut in the sagittal plane on a Microtec rotation microtome (Techno-Med GmbH, Germany) and by von Kossa / van Gieson staining. For µCT analysis, the right femur of each mouse was fixed and processed as described above. µCT scanning and analysis were performed with a voxel resolution of 10 µm as using a µCT 40 desktop cone-beam microCT (Scanco Medical, Switzerland) according to standard guidelines[4,5]. Trabecular bone was analyzed in the distal metaphysis in a volume situated 2500 µm to 500 µm proximal of the distal growth plate. A threshold value of 300 was implemented.

SUPPLEMNTARY FIGURES

Suppl. Figure 1. CD9 expression is induced in ALCAM-depleted cells. (A, B) ALCAM (green) absence was further determined by immunofluorescence analysis in H460 cells cultured on gelatin-coated slides. Immunofluoresence staining shows upregulated expression of CD9 (green) in ALCAM-KO (D) compared to parental (C) H460 cells. Higher magnification analysis reveals CD9 expression more restricted to microvilli structures in ALCAM-KO (F, arrowheads) than in parental H460 cells (E, asterisk). (G) Western blot analysis showing ALCAM expression in H460, A549, HTB56 and H1975 lung cancer cell lines. Scale bars in A, B, C, D 25µm; in E, F 10µm.

Suppl. Figure 2. Effect of ALCAM on tumor vascularisation and bone metastasis. The number of CD34-positive blood vessels in brain metastases are not altered upon ALCAM absence in either the intracranial (C, p=0.136) or intracardial (D, p=0.283) mouse models. Representative von Kossa / van

Gieson stained undecalcified spine sections from intracranial mice injected with either parental (E) or H460 ALCAM-KO (F) cells showing no tumor cell infiltration and bone damage. Intracardial injected mice show metastasis in spine sections independent of ALCAM status (G H460 parental, H H460 ALCAM-KO cells). Bone μCT analysis of femora from intracranial injected mice (I-L) revealed no difference in trabecular bone mass (BV / TV: bone volume per tissue volume) (I, p=0.9342) and cortical porosity (J, p=0.5601). In contrast, osteolytic lesion could be observed by μCT in the femora of intracardial injected mice. However, no difference between the groups in trabecular bone mass (M, p=0.4973) or cortical porosity (N, p=0.6148) could be detected, whereas the bone mineral density (Q) was decreased in H460 parental cell injected mice (p=0.043). Mean ± s.d. Scale bar in A, B: 50μm.

REFERENCES

1. Weber K, Bartsch U, Stocking C, Fehse B. A multicolor panel of novel lentiviral "gene ontology" (LeGO) vectors for functional gene analysis. *Mol Ther.* 2008; 16(4):698-706.

2. Corbeil D, Roper K, Hannah MJ, Hellwig A, Huttner WB. Selective localization of the polytopic membrane protein prominin in microvilli of epithelial cells - a combination of apical sorting and retention in plasma membrane protrusions. *J Cell Sci.* 1999; 112 (Pt 7):1023-1033.

3. Albers J, Keller J, Baranowsky A, et al. Canonical Wnt signaling inhibits osteoclastogenesis independent of osteoprotegerin. *J Cell Biol.* 2013; 200(4):537-549.

4. Bouxsein ML, Boyd SK, Christiansen BA, Guldberg RE, Jepsen KJ, Muller R. Guidelines for assessment of bone microstructure in rodents using micro-computed tomography. *J Bone Miner Res.* 2010; 25(7):1468-1486.

5. Yorgan TA, Peters S, Jeschke A, et al. The Anti-Osteoanabolic Function of Sclerostin Is Blunted in Mice Carrying a High Bone Mass Mutation of Lrp5. *J Bone Miner Res.* 2015; 30(7):1175-1183.

Figure 1

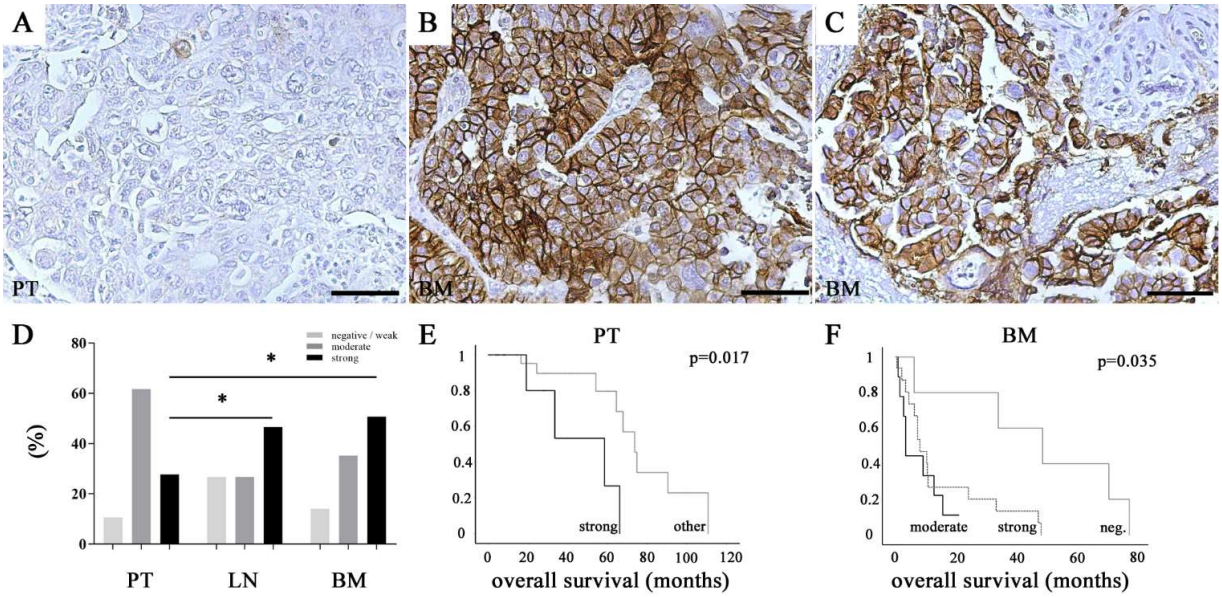
A
B
C
PT
BM
BM
D
negative / weak
moderate
strong
(%)
80
60
40
20
0
*
*
PT
LN
BM
E
PT
p=0.017
1
0.8
0.6
0.4
0.2
0
strong
other
0 20 40 60 80 100 120
overall survival (months)
F
BM
p=0.035
1
0.8
0.6
0.4
0.2
0
moderate
strong
neg.
0 20 40 60 80
overall survival (months)

Figure 2

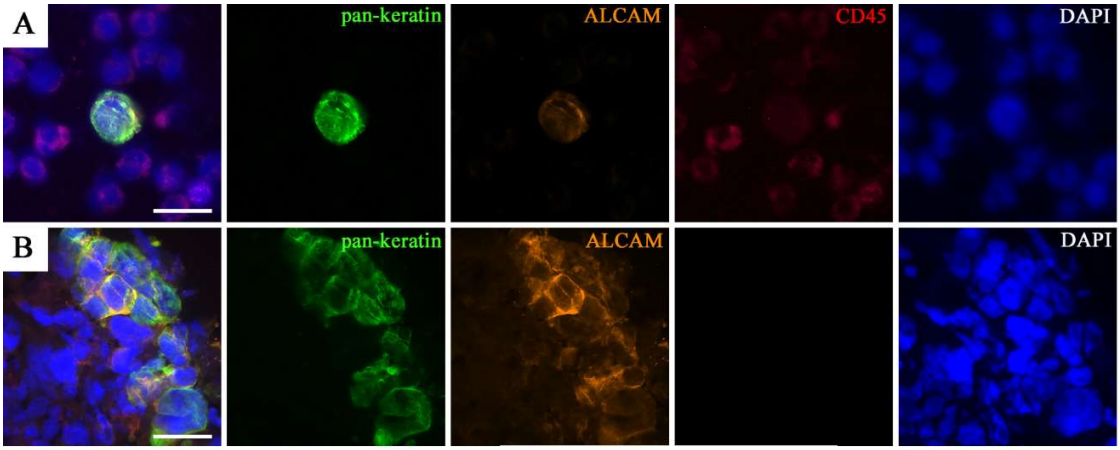

C

	CTC	BM
Patient 1	neg.	neg.
Patient 2	pos.	pos.
Patient 3	weak	weak
Patient 4	pos.	pos.

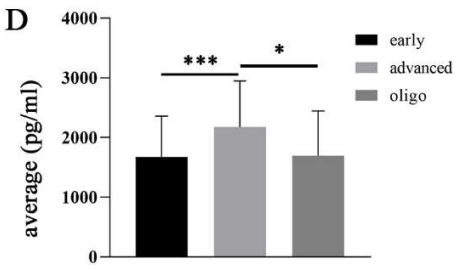

Figure 3

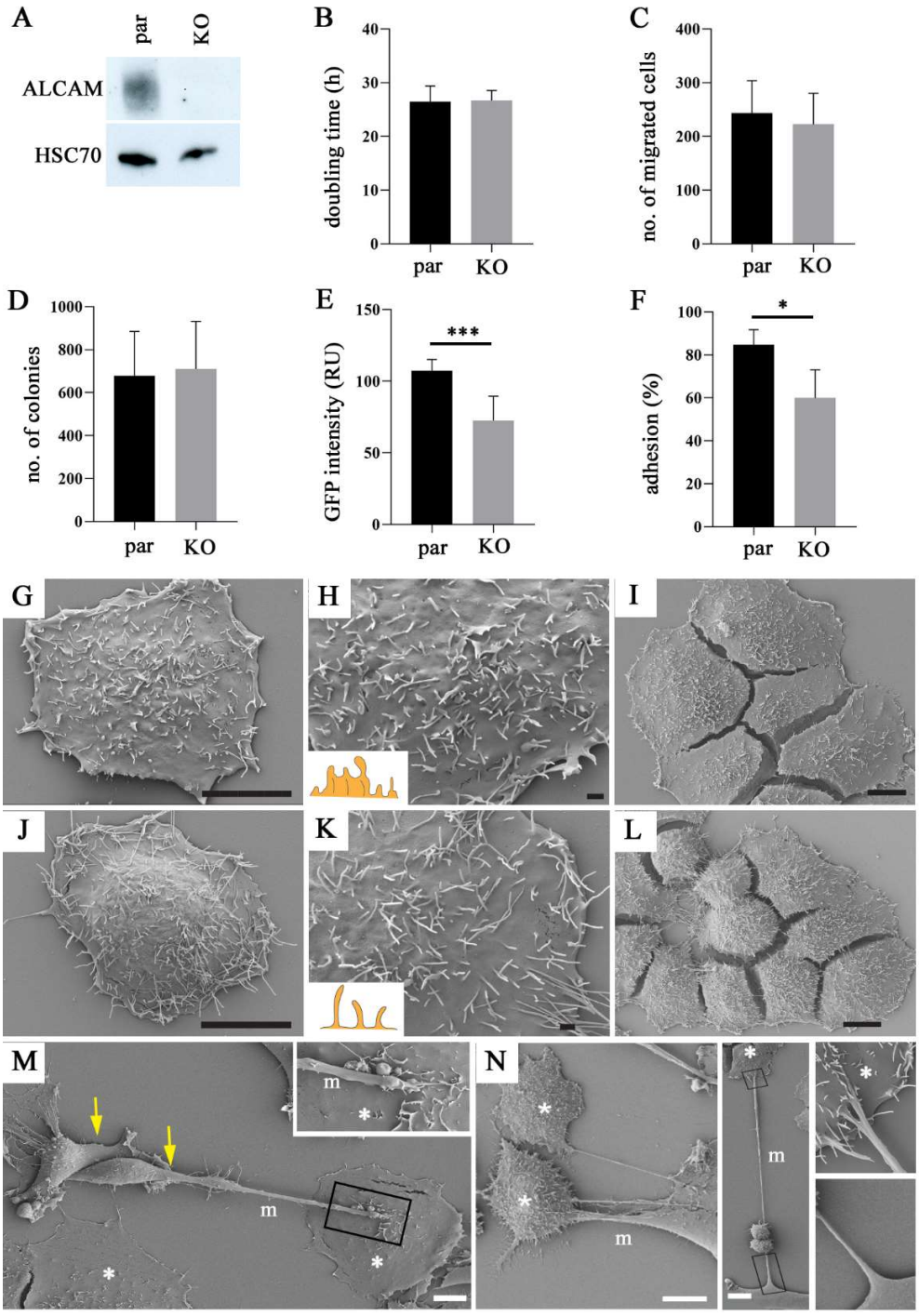
A
par
KO
ALCAM
HSC70
B
doubling time (h)
par
KO
C
no. of migrated cells
par
KO
D
no. of colonies
par
KO
E
GFP intensity (RU)
***
par
KO
F
adhesion (%)
*
par
KO
G
H
I
J
K
L
M
m
N
m
m

Figure 4

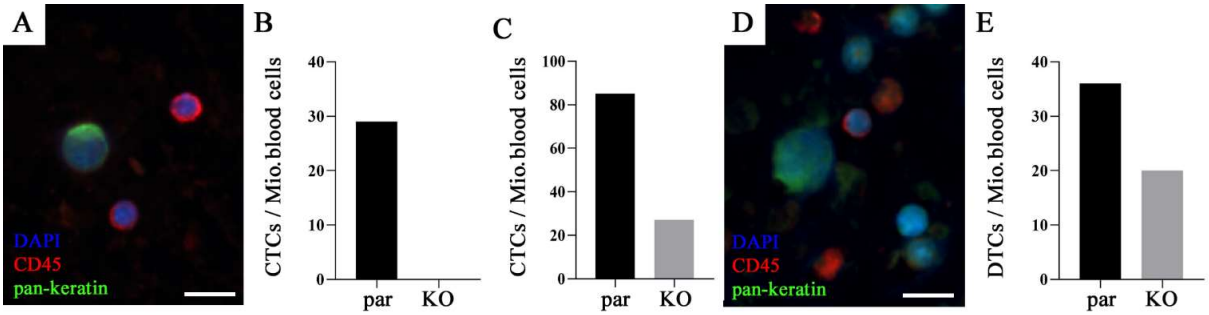
A
DAPI
CD45
pan-keratin
B
CTCs / Mio.blood cells
40
30
20
10
0
par
KO
C
CTCs / Mio.blood cells
100
80
60
40
20
0
par
KO
D
DAPI
CD45
pan-keratin
E
DTCs / Mio.blood cells
40
30
20
10
0
par
KO

Figure 5

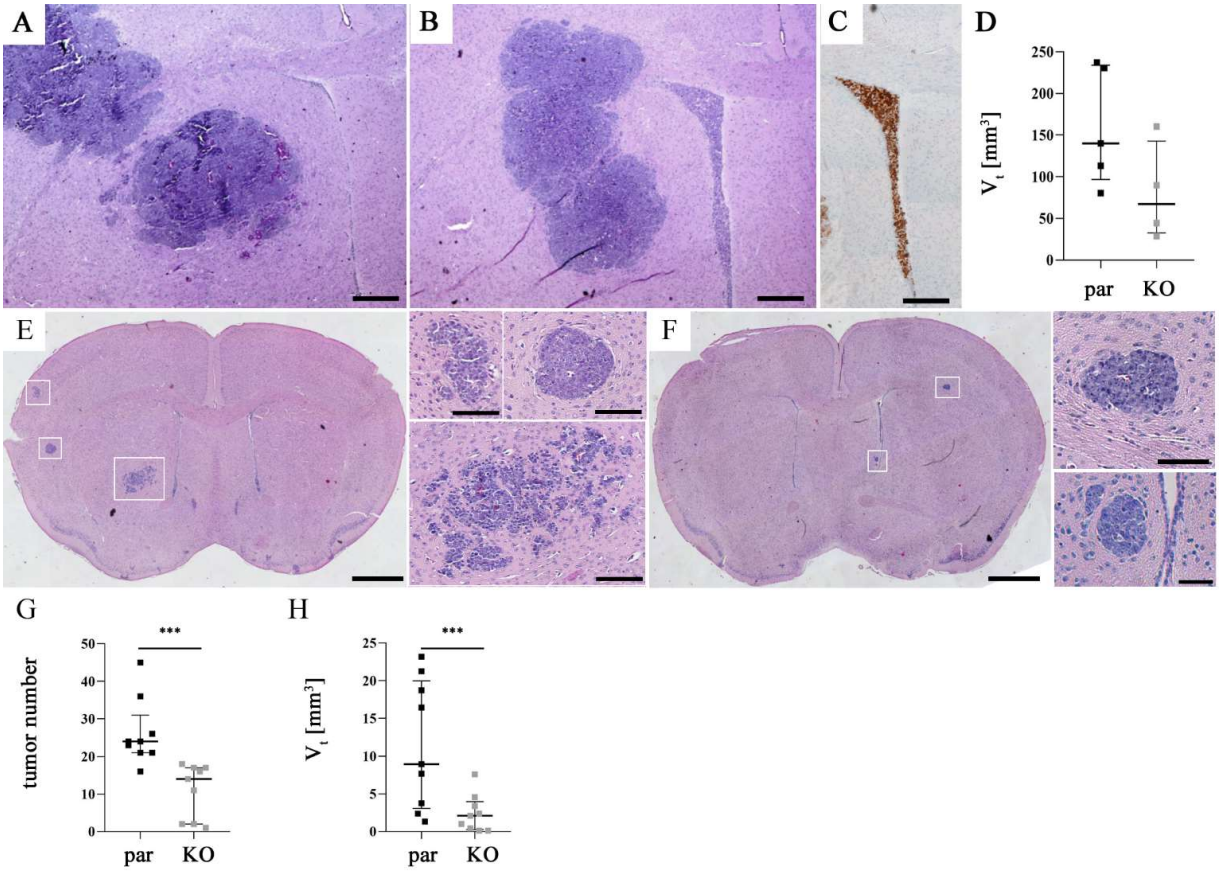
A
B
C
D
250
200
150
100
50
0
V_t [mm^3]
par
KO
E
F
G
H
***
tumor number
50
40
30
20
10
0
par
KO
***
25
20
15
10
5
0
V_t [mm^3]
par
KO

Supplementary Figure 1

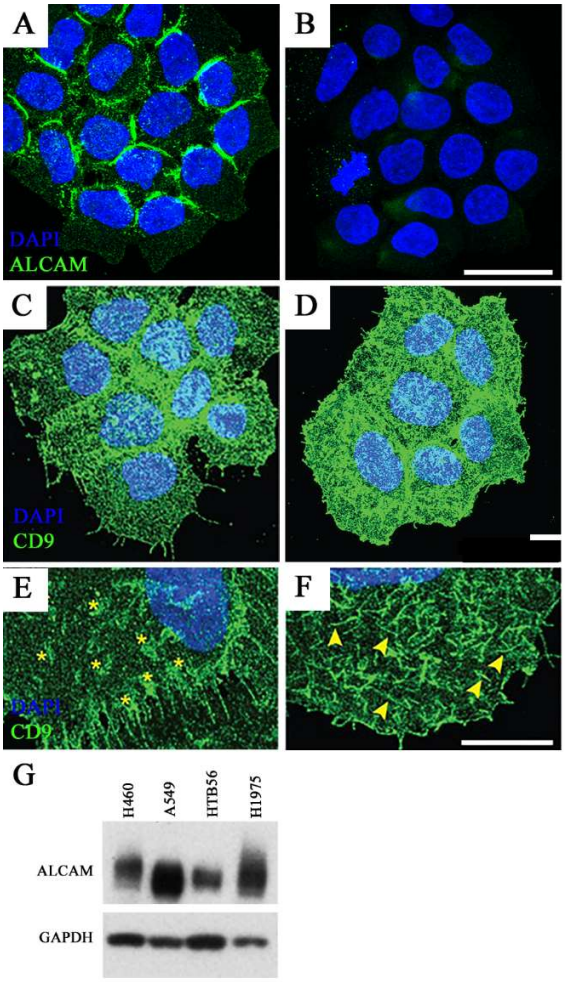

Supplementary Figure 2